Published in final edited form as:

Biofabrication. ; 11(2): 025013. doi:10.1088/1758-5090/ab078a.

Bioprinted Osteon-like Scaffolds Enhance in Vivo Neovascularization

Charlotte Piard[1,2], **Hannah Baker**[1,2], **Timur Kamalitdinov**[1,2], **John Fisher**[1,2,*]

[1]Fischell Department of Bioengineering, University of Maryland, 3121 A James Clark Hall, College Park,MD20742, United States of America

[2]Center for Engineering Complex Tissues, University of Maryland, 3121 AJames Clark Hall, College Park,MD20742, United States of America

Abstract

Bone tissue engineers are facing a daunting challenge when attempting to fabricate bigger constructs intended for use in the treatment of large bone defects, which is the vascularization of the graft. Cell-based approaches and, in particular, the use of in vitro coculture of human umbilical vein endothelial cells (HUVECs) and human mesenchymal stem cells (MSCs) has been one of the most explored options. We present in this paper an alternative method to mimic the spatial pattern of HUVECs and hMSCs found in native osteons based on the use of extrusion-based 3D bioprinting (3DP). We developed a 3DP biphasic osteon-like scaffold, containing two separate osteogenic and vasculogenic cell populations encapsulated in a fibrin bioink in order to improve neovascularization. To this end, we optimized the fibrin bioink to improve the resolution of printed strands and ensure a reproducible printing process; the influence of printing parameters on extruded strand diameter and cell survival was also investigated. The mechanical strength of the construct was improved by co-printing the fibrin bioink along a supporting PCL carrier scaffold. Compressive mechanical testing showed improved mechanical properties with an average compressive modulus of 131±23MPa, which falls in the range of cortical bone. HUVEC and hMSC laden fibrin hydrogels were printed in osteon-like patterns and cultured in vitro. A significant increase in gene expression of angiogenic markers was observed for the biomimetic scaffolds. Finally, biphasic scaffolds were implanted subcutaneously in rats. Histological analysis of explanted scaffolds showed a significant increase in the number of blood vessels per area in the 3D printed osteon-like scaffolds. The utilization of these scaffolds in constructing biomimetic osteons for bone regeneration demonstrated a promising capacity to improve neovascularization of the construct. These results indicates that proper cell orientation and scaffold design could play a critical role in neovascularization.

Keywords

osteon; bone tissue engineering; bioprinting; neovascularization; biomimetic; fibrin

[*]**Corresponding Author(s):** John P. Fisher, Fischell Family Distinguished Professor & Department Chair, Fischell Department of Bioengineering, University of Maryland, 4102A Clark Hall, 8278 Paint Branch Drive, College Park, MD 20742, Phone: 301.314.2188, jpfisher@umd.edu.

Introduction

With more than 600,000 procedures performed in the United States annually, bone is the second most transplanted tissue [1]. Although autografts and allografts are the current standards in orthopedic reconstructive surgeries and have proven successful, they present significant drawbacks [2]. Bone tissue engineering is a promising alternative, providing bone substitute that can potentially eliminate donor site morbidity associated with autografts or immune rejection and pathogens transfers associated with allografts [3]. However bone tissue engineers are facing a daunting challenge when attempting to fabricate bigger constructs intended for use in the treatment of large bone defects: the vascularization of the graft. Vasculature is a requirement when engineering most tissues in order to provide nutrients, factors and oxygen to avoid tissue necrosis [4]. Many investigators have successfully demonstrated the use of different strategies to develop vascular structures, including growth factor delivery [5], channeled scaffolds [6], perfusion bioreactors [7], cell cocultures [8], cell functionalization [9], and *in vivo* systems [10].

Cell-based approaches and, in particular, the use of *in vitro* coculture of human umbilical vein endothelial cells (HUVECs) and human mesenchymal stem cells (hMSCs) has been one of the most explored options [8, 11–12]. In cortical bone, both cell populations, osteogenic and vasculogenic, are arranged in a well-defined pattern, called osteons [13]. Each osteon is composed of concentric bone-cells containing layers (lamellae) surrounding the Haversian canal, a narrow central channel, which contain small blood vessels. One attempt to recreate osteon-like structures used electrospun gelatin/PLLA rods seeded with osteoblasts [14]. However, cell infiltration in this avascular scaffolds was hindered by the tight nanofibrous network resulting in cell apoptosis.

To address this shortcoming, we present in this paper an alternative method to mimic the spatial pattern of HUVECs and hMSCs found in native osteons based on the use of extrusion-based 3D bioprinting (3DP). 3DP offers an efficient tool for accurate fabrication of biomaterial scaffolds with tunable properties [15]. 3DP using a three-axis dispensing system, which builds 3D constructs by extruding fibers of cell-laden materials in a layer-by-layer fashion, as directed by computer-aided design (CAD) model. Fibrin is a natural polymer known to support wound healing by inducing angiogenesis and promoting cell attachment and proliferation, and therefore an attractive matrix for stem cell differentiation and tissue engineering [16]–[18]. Although fibrin has shown potential *in vitro* in promoting osteogenesis, it lacks the mechanical strength required for bone tissue engineering [19]. The co-printing of a solid mechanically strong and porous matrix, such as polycaprolactone (PCL) along a softer biocompatible hydrogel into which the embedded cells can proliferate and differentiate is an alternative strategy [20]. PCL is biocompatible and exhibits a slow biodegradation rate that can maintain mechanical stability long enough to allow new bone formation [21].

In the present study, the overall objective was to develop a 3DP biphasic osteon-like scaffold, containing two separate osteogenic and vasculogenic cell populations encapsulated in a fibrin bioink in order to improve neovascularization. To this end, the first objective was to optimize the fibrin bioink to improve the resolution of printed fibers and ensure a

reproducible printing process; the influence of printing parameters on extruded fiber diameter and cell survival was also investigated. The second objective was to improve the mechanical strength of the construct by co-printing the fibrin bioink along a supporting PCL carrier scaffold. Finally, HUVEC and hMSC laden fibrin hydrogels were printed in osteon-like patterns and cultured *in vitro*. Biphasic scaffolds seeded with rat aortic endothelial cells and MSCs were implanted subcutaneously in rats. Results showcase the capacity of our 3DP biphasic construct to provide accurate physical cues for large-scale vascularized bone.

Material and Methods

Cell Culture

L929 cells (ATCC, Manassas, VA) were cultured as per the manufacturer's specifications with Minimum Essential Medium (Life Technologies, Frederick, MD) and 10% horse serum (Life Technologies). Prior to printing, cells were passaged using Trypsin/EDTA and encapsulated in fibrin bioink (two densities were examined, 2×10^6 cells/ml and 10×10^6 cells/ml).

hMSCs (Lonza, Walkersville, MD) were cultured in control media consisting of Dulbecco's Modified Eagle's medium (DMEM, Gibco, Carlsbad, CA) supplemented with 10% fetal bovine serum (Gibco), 1.0% v/v penicillin/streptomycin (Gibco), 0.1 mM non-essential amino acids (Gibco), and 4 mM L-glutamine (Gibco as per the manufacture's specifications). Cells were expanded on tissue culture polystyrene flasks with media changes every 3 days, and grown to 80% confluency before being passaged using trypsin/EDTA. Cells at passage P2 were used for the experiments.

HUVECs (Lonza) were cultured in EBM-2 Basal Medium (Lonza) supplemented by EGM-2 SingleQuot Kit. Rat primary aortic endothelial cells (RAECs) were purchased from Cell Biologics (Chicago, IL) and cultured according to manufacturer instructions. Rat MSCs (rMSCs) were purchased from RD Systems (Minneapolis, MN) and cultured in osteogenic media for 7 days prior to implantation. The osteogenic media was formulated by supplementing growth media with 100 nM dexamethasone (Sigma, St. Louis, MO), 10 mM β-glycerophosphate (Sigma), and 173 mM ascorbic acid (Sigma). Cells were expanded on tissue culture polystyrene flasks with media changes every 3 days, and grown to 80% confluency before being passaged using trypsin/EDTA. Cells at passage P4 were used for the experiments.

Fibrin Hydrogel Preparation and Characterization

Fibrin Bioink.—Fibrinogen and thrombin from bovine plasma, and gelatin type I were purchased from Sigma. Type A porcine gelatin (300g Bloom) was purchased from Sigma. The bioink was prepared by mixing different ratios of fibrinogen and gelatin and heating to 60°C for 15 min. The hydrogel samples were printed using an extrusion based bioprinter (3D-Bioplotter; EnvisionTEC; Germany). All printing supply (30cc barrel and 200 μm/400 μm precision tips) were purchased from Nordson EFD (RI, USA). The fibrin bioink was loaded into the low-temperature printer head and allowed to equilibrate for 30 min at a 22°C. Printed constructs were crosslinked in 100 U thrombin for 30 min. The printer took

successive images of each layer during printing, allowing quantification of strand diameter in each layer.

Swelling experiment.—For each bioink formulation, nine samples per group were printed and crosslinked. Each 10 mm by 10 mm sample was printed using a 200 μm tip, and fibers were spaced every 200 μm. Pictures were taken before and after 24 h incubation in PBS at 37°C. Images were analyzed using ImageJ to calculate strand diameter and pore area. Swelling was calculated by dividing the average porosity of a sample post-printing by the average porosity of the same sample after incubation.

Cell Viability Assay.—Mouse fibroblast, L929, were used to assess in vitro viability, as per ISO standard 10993–5. Cell viability was assessed using a Live/Dead assay (Invitrogen) following the manufacturer's protocol. Briefly, 6 samples per group were incubated with 2 μM ethidium homodimer and 4 μM calcein AM for 1 h. Dead control were incubated in 70% methanol (Sigma) for 15 min prior to Live/dead staining. Fluorescent images were taken using a confocal microscope (Leica SP5 X). Five digital images per samples, with each an area of 1 $mm^{2,}$ were processed in ImageJ. A resulting percentage of cell viability was calculated from the ratio of the number of live cells divided by the total number of cells.

Evaluation of Fibrin Hydrogels.—Shear stress and viscosity measurements as a function of shear rate of the fibrin bioink were obtained at 22°C (printing temperature) using an AR2000 stress controlled rheometer (TA Instruments, Newark, DE) with a plate-plate geometry. A Q800 Dynamic Mechanical Analyser (TA Instruments LLC, Delaware, USA) was used to evaluate the compressive modulus of fibrin hydrogels. The compressive stress-strain was obtained at a strain rate of 1mm/min at room temperature.

PCL Carrier Scaffold Fabrication and Characterization

Computational Modeling.—Scaffolds were designed with 3D solid modeling CAD software (Solidworks 2015). Circular cross-sections were swept along a pattern mimicking the Bioplotter needle path during printing to make a uniformly porous structure. CAD models corresponding to various extruder needle sizes (200 and 400 μm) and inner cylinder diameters (2, 4, and 6 mm) were designed. Computational fluid dynamic analysis was performed using Solidworks Flow Simulation Module. Briefly, the scaffold models were enclosed in a hollow cylinder to allow for the establishment of the computational domain with the inlet perfusing water at a fully developed, laminar, volumetric flowrate of 100 mm^3/s at 37°C through the bottom of the scaffold and the outlet representing environmental pressure at the top end of the scaffold.

PCL Samples Preparation.—Scaffolds, with a dimension of 10 mm in diameter and 5 or 10 mm in height, were fabricated using a commercial 3DP system with corresponding cartridges and needles (3D Bioplotter, EnvisionTEC, Gladbeck, Germany). PCL (MW 43000, Polysciences, Warrington, PA) was loaded into a high temperature print head and heated at 120°C for 30 min prior to printing. Strands were extruded at a pressure of 5 bar and speed of 2 mm/s to form scaffolds.

Scanning Electron Microscopy (SEM).—For morphology observation of internal structures, samples were imaged by a field emission gun scanning electron microscope (Hitachi SU-70) at 5 kV. Images were analyzed using ImageJ to calculate pore size and strand diameter and to determine printing accuracy.

Compressive Mechanical Testing.—Compressive mechanical analysis was performed on four samples per group using an Instron mechanical testing system (33R/4465, Norwood, MA). All tests were performed using a high-capacity load cell (5000 N). Samples were compressed at a displacement rate of 2 mm/min, and experimental values were recorded every 10 ms. Compression was maintained until a drop of at least 60% in force was measured. Engineering stress and strain were calculated based on original cross-sectional area and height, respectively, which were then used to compute compressive modulus, 1% offset yield stress, and ultimate compressive stress.

In vitro and In vivo evaluation

Scaffolds Preparation.—Scaffolds for *in vitro* and *in vivo* evaluation were fabricated using a commercial 3D printing system (3D Bioplotter, EnvisionTEC, Gladbeck, Germany). For both experiments, cells were passaged, suspended in media and centrifuged to form a pellet. After aspiration of the supernatant, the pellet was then suspended in fibrin bioink by manual pipetting, until the solution was homogenous and all clumps were broken down. All fibrin samples, control and experimental, were about 1 mm in thickness and 2.5 mm in diameter.

For *in vitro* evaluation, fibrin bioink encapsulating either 2×10^6 hMSCs/mL or 3×10^6 HUVECs/mL were loaded into separate print heads and were heated to 22°C for 30 min prior to printing. Control groups consisted of fibrin bioink casted within the barrel of a 3 mm diameter syringe, and contained a suspension of hMSCs and HUVECs (ratio 3:1) at a density of 2×10^6 cells/mL. The ratio was calculated based on the actual volume of ECs and MSCs bioinks used by the Bioplotter to print the experimental samples (19μL and 73μL respectively, for a print comprise of 25 osteons).Once gelled, control samples were casted out of the syringe using the plunger. All scaffolds were crosslinked into 100 U thrombin for 30 min before being transferred to appropriate culture media and incubated at 37°C. Media was changed every 2 days. For in vivo experiments, fibrin bioink encapsulating 2×10^6 rMSCs/ml or 3×10^6 RAECs/ml and PCL were loaded into separate print heads and were heated to 22°C and 120°C respectively, for 30 min prior to printing. Control groups consisted of printed PCL base and a casted fibrin bioink disc containing either a suspension of rMSCs or a suspension of rMSCs and RAECs (ratio 3:1) at a density of 2×10^6 cells/ml. All scaffolds were allowed to crosslink for 30min in 100 U thrombin before subdermal rat implantation.

DNA quantification Assay.—Cell samples from each group (n=9) were isolated from fibrin hydrogels by dissolution in 1 mg/mL collagenase (Sigma) for 120 min at 37°C and a cell pellet was formed by centrifugation and washed with PBS three times. Total DNA was isolated using DNeasy Blood and Tissue Kit (Qiagen) according to the manufacturer

instructions. DNA content was quantified using the PicoGreen DNA assay (Invitrogen) following manufacturer's instructions.

Quantitative reverse transcriptase polymerase chain reaction (rt-PCR).—Total RNA was isolate using RNeasy Plus Mini Kit (Qiagen), following the supplier's protocol (n=9). Reverse transcription was performed using TaqMan Reverse Transcription reagents (Applied Biosystems) following the supplier's protocol. qRT-PCR was performed using TaqMan PCR Master mix and Taqman Gene Expression Assays for alkaline phosphatase (ALP), bone morphogenetic protein-2 (BMP2), vascular endothelial growth factor-A (VEGFA) and platelet and endothelial cell adhesion molecule-1 (PECAM1). Quantification of target gene expression was calculated relative to the reference glyceraldehyde 3-phosphate dehydrogenase (GAPDH) gene. The mean minimal cycle threshold values (Ct) were calculated from triplet reactions.

Animal Implantation.—The Institutional Animal Care and Use Committee of the University of Maryland approved the study (protocol number R-MAY-18–26), and all animals were treated in accordance with the Guide for the Care and Use of Laboratory Animals. The experiment was conducted in 6 male adult Sprague Dawley rats. A small incision was made on the back of each animal, and one scaffold from each group was implanted in the subdermal space. At 7 and 14 days post implantation, 3 animals were euthanized and the samples and surrounding tissue were explanted. Each explanted tissue sample was preserved in paraformaldehyde (4%) for histological analysis.

Histological Analysis.—Explanted tissue samples were processed, embedded in paraffin and sliced (15 μm slides) by Histoserv, Inc. (Germantown, MD). For histological evaluation, sections were stained by Masson's Trichrome staining and Von Kossa staining, to demonstrate deposits of calcium or calcium salts. Von Kossa calcium positive control slides (placenta) were purchased from Newcomer Supply (Middleton, WI). Images were analyzed using ImageJ to quantify collagen surface area, cell surface area, and the number of blood vessels per area. Area refers here to the area of the picture, to which the empty area (void left by the PCL scaffold) were subtracted. To quantify collagen surface area (stained blue) and cell surface area (stained purple), first hues were adjusted using the function Adjust/ Color Threshold to isolate either blues or purples. The pictures were then made binary (Process/Binary), and the black surface area was measured. Cell or collagen surface area were obtained by subtracting the area occupied by the scaffolds fibers to the black surface area. Blood vessels were identified as tubular structure with dark purple rim, filled with erythrocytes (stain light purple/red).

Statistical Analysis

Data was analyzed using single factor analysis of variance (ANOVA) followed by Tukey's Multiple Comparison Test assuming normal data distribution with a confidence of 95% ($p<0.05$).

Results and Discussion

3D printed fibrin bioink

3D printing offers an efficient tool for accurate fabrication of biomaterial scaffolds with tunable properties and defined architecture. The first objective of this work was to optimize the fibrin bioink to improve the resolution of printed fibers, and to understand the influence of printing parameters on extruded fiber diameter and cell survival in order to ensure a reproducible printing process.

Because of their mechanical degradation properties (i.e. fibrin breaks down with shear), fibrin hydrogels are not good candidates for pressure based extrusion printing. A composite hydrogel consisting of fibrinogen and gelatin was then prepared, using gelatin as a support material during the printing process, which then will leached out into the media (see Supplemental Figure I). We tested two concentrations (5w/v% and 10w/v %) of each component to achieve proper printing resolution. Each group of bioink was extruded to form a rectangular lattice, with defined fiber diameter and pore size. Pictures of each printed samples were taken immediately after printing and 24h after crosslinking in thrombin and incubation at 37°C to allow the gelatin to leach out (Figure Ia). All of the images were then analyzed to measure changes in pore size. The bioink containing 10w/v% fibrinogen and 5w/v% gelatin had the lowest degree of either swelling or shrinking (Figure Ib) which is ideal, and therefore was used for the remainder of the experiments. The results shown in Figure Ib can be explained by two phenomena. First, a high concentrations of fibrinogen has been shown to result in fibrin gels with an increased number of fibrin fibers and decreased porosity, which therefore do not absorb as much water as gels with lower fibrinogen concentrations [17]. Second, gelatin was used here as a thickener agent and therefore was not modified and crosslinked. The gelatin contained in the sample was leaching out into the incubation media, resulting in a loss of material in the sample.

Prior to printing full-size constructs, parameters influencing cell viability were investigated in order to select the most appropriate conditions to construct a highly viable cell-laden scaffold. Fibers of bioink seeded with L929 cells were extruded at variable pressure (1.5 to 3.5 bar), needle type (conical or cylindrical), and needle diameter (250μm and 400μm) to study the effect of pressure and needle characteristics on cell viability directly after printing. Extruded fibers were stained with Live/Dead and imaged (Figure Ic). Images were processed and dead or live cells counted to quantify cell viability. Across all groups and for any pressure, cell viability was greater than to 70% (Figure Id). For all tested needles, higher extrusion pressure resulted in decreased cell viability. Cell viability was dependent on needle type, with higher cell viability for conical needles at low pressure (<2 bar). However for higher pressures (>2.5 bar), cell viability observed for cylindrical needles was significantly ($p<0.05$) higher than with conical needles. To understand the discrepancy between two needle types, finite elements simulations were performed (Supplemental Figure II). The simulation demonstrated that for low pressure, higher shear stresses were shown for conical needles, but were only observed proximal to the fluid outlet, limiting exposure to high shear stress to this region. On the other hand, shear stresses in cylindrical needles were lower but for an increased passage length. However, at higher pressure (>2.5 bar), as flow velocity

increased, the passage time of cells in this high shear region is reduced and the limited exposure to shear stress in conical needles cannot make up for the higher shear stresses induced.

The accuracy of a 3D printed sample depends on the accuracy of the extruded fibers. Fibers should be round and their diameter should theoretically match the inner diameter of the extrusion needle. The effects of extrusion pressure, plotting speed, and cell density using different needle size, on extruded fibers diameter, and therefore printing accuracy, are shown in Figure Ie (Supplemental Figure II). Increased pressure, and decreased speed resulted in larger fibers diameter, which was expected. The incorporation of cells altered the rheological properties (Supplemental Figure III), which was correlated with fiber diameters. While using a 400μm needle, results showed decreased fiber diameter with increased cell density, with smaller fibers (i.e. more viscous bioink) observed with the highest cell density. However, while using a 250μm needle, results showed no correlation between fibers diameter and cell density. This indicated that the viscosity of the low cell density bioink changed in function of the applied shear stress between needle sizes.

PCL Carrier Scaffold Characterization.

The second objective was to improve the mechanical strength of the construct by co-printing the fibrin bioink along a supporting PCL carrier scaffold. Tissue engineering scaffolds must retain sufficient mechanical properties to fulfill the requirements of structural integrity once implanted in vivo. Accordingly, we considered whether our osteon-like constructs had mechanical properties similar to that of bone. Dynamic mechanical analysis performed on fibrin hydrogels showed an elastic modulus of 0.7±0.3MPa under compression. However, cortical bone compressive strength is in the range of 100–150MPa [22]. In order to improve the mechanical strength of the construct, we designed and 3D printed PCL carrier scaffolds that would be co-printed along the fibrin bioink and would encase several fibrin hydrogels (Figure IIa). Several PCL carrier scaffolds were 3D printed, with defined pore size, fiber diameter, center post and variable porosity (Figure IIb). Sufficiently high porosity and a suitable pore size are required for spreading of cells and nutrients throughout the structure. An optimal pore size for bone tissue engineering scaffolds is not well defined, however pore sizes between 100 and 400μm are considered optimal for osteoconduction, and pore sizes greater than 300μm have been shown to enhance bone formation via vascularization [23], [24]. In order to evaluate printing accuracy, SEM images (Figure IIb) of the 3D printed constructs were analyzed in order to quantify the resulting pore size and fiber diameter. Across, all printed constructs, results showed that printed fibers were on average 9.6±0.4% bigger that the designed ones, resulting in pores on average 18.2±1.7% smaller, due to spreading and thermal expansion of the PCL matrix during 3D printing. These results were taken into account when designing PCL 3D printed scaffolds for later experiments.

Computational modeling of flow was performed and showed a homogeneous and sufficient fluid distribution throughout the scaffold, with minimum shear stress (Figure IIc). Finally, compressive mechanical testing was performed on 3D printed PCL scaffolds. Figure IId shows a typical stress/strain curve from compression testing, with an initial increase in stress at low strain followed by a plateau region, with fluctuations. These fluctuations could be

attributed to the successive collapse of each layers under compression. The compressive moduli of the porous scaffolds were quantified from the initial slope of the stress–strain curve in Figure IId. All the PCL scaffolds showed improved mechanical properties with an average compressive modulus of 130.93±22.74MPa, which falls in the lower range of cortical bone [22].

In Vitro and In Vivo Evaluation of Osteon-like Scaffolds.

The third objective of this work was to test the osteogenic and angiogenic potential of osteon-like scaffolds, and demonstrated that a biomimetic approach could enhance neovascularization of the graft. Constructs were 3D printed using the Bioplotter. As shown in figure IIIa and IIIb, the osteon-like unit had a concentric triple-ring structure with an outer diameter of 2.5 mm. A set of two bioink were used: one encapsulating hMSCs for the outer rings and one encapsulating HUVECs to recreate the Harversian canal in the center. After 14 days of in vitro culture, cells were retrieved and DNA and RNA were collected. The DNA quantification assay showed a significantly higher ($p<0.05$) DNA concentration in the printed samples compared to the casted samples (Figure IIIc). In addition, a significant increase ($p<0.05$) in DNA concentration over the 14 days was found for the printed samples, while the casted samples showed no significant changes ($p=0.084$). Scaffolds were stained using Live/Dead to assay cell viability after 7 and 14 days of culture (Figure IIIe). Cell viability was not significantly different ($p=0.071$) between control and experimental groups. After 14 days, cell viability was 94.8±2.8% for the printed samples. Rt-PCR showed an increase in gene expression of BMP2, ALP, VEGFA and PECAM1 in both groups after 14 days (Figure IIId). However, while rt-PCR showed no significant difference in gene expression of osteogenic markers ($p=0.098$), a significant fold change ($p<0.05$) in mRNA of angiogenic markers was observed.

In vivo experiments were performed in order to demonstrate the ability of the construct to successfully integrate with the host tissue and assess the angiogenic potential of the scaffolds. Osteon-like samples, as well as MSCs/ECs casted controls, were implanted subcutaneously in rats (Figure IVa), with enough distance between them to be retrieve easily: the MSCs only control was implanted cranially, the MSCs/ECs control caudally and the 3D printed samples in the middle. After 14 days, the samples were retrieved. From simple visual inspection, experimental samples appeared to have a darker red color indicative of potential vascularization (Figure IVb). Further histological analyses were performed using Masson's trichrome and Von Kossa (for mineralization) stains. No signs of inflammation (large fibrous capsule, giant cells) were observed in all groups. Masson's trichrome stain showed a clear qualitative difference between samples (Figure IVc). In the control sample, the fibrin hydrogel was still visible and the delimitation from surrounding tissue is clear. Cell invasion within the hydrogel had not reached the PCL carrier scaffolds, and few blood vessels were visible. The fibrin hydrogel from the 3D printed sample exhibited a stronger blue staining, suggesting that more collagen had been deposited. The same observation were made with the Von Kossa stained samples (Supplemental Figure IV): all groups showed increased mineralization between day 7 and day 14, but the 3D printed samples exhibited the most increase.

Quantitative assessment was performed using Image J. The percentage area of each picture covered by collagen or cells was measured and averaged. The number of blood vessels per area was also counted and averaged. No statistical difference in collagen deposition was observed between the three groups after 7 days. However, after 14 days of *in vivo* culture, both groups containing ECs had a statistically higher collagen deposition than the MSCs only control. After 14 days of *in vivo* culture no significant difference ($p=0.087$) in cell density between groups was observed. However, cell infiltration was more pronounced in the 3DP osteon-like groups, as shown by a statistically higher surface area ($p<0.05$) covered by cells after 7 days of culture. Finally, after 14 days of culture, blood vessels were observed throughout the scaffolds, and a significant increase ($p<0.05$) in the number of blood vessels per area in 3DP osteon-like samples was observed.

In both the mixed and osteon-like scaffolds, the co-culture of ECs and MSCs improved the deposition of collagen, one marker of osteogenesis, and neovascularization. Numerous studies on ECs/MSCs coculture have been demonstrated to achieve enhanced cellular signaling. Both cell populations are known to secrete specific growth factors that are beneficial for mutual growth and differentiation for each other. MSCs promotes neovascularization by secreting pro-angiogenic growth factor such as Ang-1, FGF-2 and, VEGF likely through paracrine communication between EPCs and MSCs, which simulates EPCs proliferation and differentiation[25]–[27]. In return, EPCs secrete osteogenic growth factors such as insulin growth factor 1, and BMP-2, promoting MSCs differentiation [28]–[30]. In addition, osteon-like scaffolds showed significantly higher cell infiltration and neovascularization within the construct than the two other control groups. MSCs paracrine factors production and release has been shown to vary with the substrate microarchitecture, stiffness or composition [31]–[33]; although it remains to be proved, we contend that the specific respective patterning of cells, in this case in the shape of osteons, could also affect paracrine signaling or other cell-cell communications, and result in an improved neovascularization. Thus, further experiments are warranted to explain the observed phenomena, and relevant research is progressing in our laboratory. In addition, this osteon-like scaffold could be further optimized to improve its biomimetic characteristic, for example scaling by incorporating a non-organic phase (hydroxyapatite) to the bioink.

Conclusion

In the present study, we demonstrated the successful fabrication of a novel 3DP fibrin-PCL composite scaffold, with mechanical strength comparable to bone, a stable swelling behavior and cell bioactivity for the construction of biomimetic structures. Using 3D printing technologies, bioinks were patterned into varied geometries and with controlled dimensions, in order to recreate an optimal microenvironment mimicking the native natural cell pattern found in bones, to form a simplified model of osteons. Most importantly, the utilization of these scaffolds in constructing biomimetic osteons for bone regeneration demonstrated a promising capacity to improve neovascularization of the construct. These results indicates that proper cell orientation and scaffold design could play a critical role in neovascularization. This biomimetic osteon-like construct holds potential to be develop as scaffolds in vascularized bone tissue engineering. In addition, advancements in the field of

3D printing, and a higher level of precision, will allow the printing of ever more biomimetic structures.

Supplementary Material

Refer to Web version on PubMed Central for supplementary material.

Acknowledgement

This work was supported by the U.S. National Institutes of Health under Award No. R01 EB014946 and by the National Institute of Biomedical Imaging and Bioengineering/ National Institute of Health (NIBIB/NIH) Center for Engineering Complex Tissue P41 EB023833. The authors would also like to thanks Dr. Srinivasa Raghavan's laboratory at the University of Maryland for their help conducting rheological evaluation of the fibrin bioink.

References

[1]. Van Heest A, Swiontkowski M, Leinberry C, Cohen M, and Jupiter J, "Bone-graft substitutes," Lancet, vol. 353, pp. S28–S29, 4 1999.

[2]. Zimmermann G, Moghaddam A, A.-B. T. P. F. S. Group, and et al., "Allograft bone matrix versus synthetic bone graft substitutes.," Injury, vol. 42 Suppl 2, pp. S16–21, 9 2011. [PubMed: 21889142]

[3]. Mistry AS and Mikos AG, "Tissue Engineering Strategies for Bone Regeneration," Springer Berlin Heidelberg, 2005, pp. 1–22.

[4]. Fiedler T, Belova IV, Murch GE, Poologasundarampillai G, Jones JR, Roether JA, and Boccaccini AR, "A comparative study of oxygen diffusion in tissue engineering scaffolds," J. Mater. Sci. Mater. Med, vol. 25, no. 11, pp. 2573–2578, 11 2014. [PubMed: 25016936]

[5]. Huang Y-C, Kaigler D, Rice KG, Krebsbach PH, and Mooney DJ, "Combined Angiogenic and Osteogenic Factor Delivery Enhances Bone Marrow Stromal Cell-Driven Bone Regeneration," J. Bone Miner. Res, vol. 20, no. 5, pp. 848–857, 12 2004. [PubMed: 15824858]

[6]. Radisic M, Malda J, Epping E, Geng W, Langer R, and Vunjak-Novakovic G, "Oxygen gradients correlate with cell density and cell viability in engineered cardiac tissue," Biotechnol. Bioeng, vol. 93, no. 2, pp. 332–343, 2 2006. [PubMed: 16270298]

[7]. Ball O, Nguyen B-NB, Placone JK, and Fisher JP, "3D Printed Vascular Networks Enhance Viability in High-Volume Perfusion Bioreactor," Ann. Biomed. Eng, vol. 44, no. 12, pp. 3435–3445, 12 2016. [PubMed: 27272210]

[8]. Nguyen B-NB, Moriarty RA, Kamalitdinov T, Etheridge JM, and Fisher JP, "Collagen hydrogel scaffold promotes mesenchymal stem cell and endothelial cell coculture for bone tissue engineering," J. Biomed. Mater. Res. Part A, vol. 105, no. 4, pp. 1123–1131, 4 2017.

[9]. Egaña JT, Fierro FA, Krüger S, Bornhäuser M, Huss R, Lavandero S, and Machens H-G, "Use of Human Mesenchymal Cells to Improve Vascularization in a Mouse Model for Scaffold-Based Dermal Regeneration," Tissue Eng. Part A, vol. 15, no. 5, pp. 1191–1200, 5 2009. [PubMed: 18925832]

[10]. Kneser U, Polykandriotis E, Ohnolz J, Heidner K, Grabinger L, Euler S, Amann KU, Hess A, Brune K, Greil P, StüRzl M, and Horch RE, "Engineering of Vascularized Transplantable Bone Tissues: Induction of Axial Vascularization in an Osteoconductive Matrix Using an Arteriovenous Loop," Tissue Eng, vol. 12, no. 7, pp. 1721–1731, 7 2006. [PubMed: 16889503]

[11]. Dahlin RL, Gershovich JG, Kasper FK, and Mikos AG, "Flow Perfusion Co-culture of Human Mesenchymal Stem Cells and Endothelial Cells on Biodegradable Polymer Scaffolds," Ann. Biomed. Eng, vol. 42, no. 7, pp. 1381–1390, 7 2014. [PubMed: 23842695]

[12]. Ma J, van den Beucken JJJP, Yang F, Both SK, Cui F-Z, Pan J, and Jansen JA, "Coculture of Osteoblasts and Endothelial Cells: Optimization of Culture Medium and Cell Ratio," Tissue Eng. Part C Methods, vol. 17, no. 3, pp. 349–357, 3 2011. [PubMed: 20932081]

[13]. Tertuliano OA and Greer JR, "The nanocomposite nature of bone drives its strength and damage resistance," Nat. Mater, vol. 15, no. 11, pp. 1195–1202, 8 2016. [PubMed: 27500809]

[14]. Andric T, Sampson AC, and Freeman JW, “Fabrication and characterization of electrospun osteon mimicking scaffolds for bone tissue engineering,” Mater. Sci. Eng. C, vol. 31, no. 1, pp. 2–8, 1 2011.

[15]. Kang H-W, Lee SJ, Ko IK, Kengla C, Yoo JJ, and Atala A, “A 3D bioprinting system to produce human-scale tissue constructs with structural integrity,” Nat. Biotechnol, vol. 34, no. 3, pp. 312–319, 2 2016. [PubMed: 26878319]

[16]. Chung E, Rytlewski JA, Merchant AG, Dhada KS, Lewis EW, and Suggs LJ, “Fibrin-based 3D matrices induce angiogenic behavior of adipose-derived stem cells.,” Acta Biomater, vol. 17, pp. 78–88, 4 2015. [PubMed: 25600400]

[17]. Janmey PA, Winer JP, and Weisel JW, “Fibrin gels and their clinical and bioengineering applications,” J. R. Soc. Interface, vol. 6, no. 30, pp. 1–10, 1 2009. [PubMed: 18801715]

[18]. An SSA and Rajangam SSA, “Fibrinogen and fibrin based micro and nano scaffolds incorporated with drugs, proteins, cells and genes for therapeutic biomedical applications,” Int. J. Nanomedicine, vol. 8, p. 3641, 9 2013. [PubMed: 24106425]

[19]. Kneser U, Voogd A, Ohnolz J, Buettner O, Stangenberg L, Zhang YH, Stark GB, and Schaefer DJ, “Fibrin gel-immobilized primary osteoblasts in calcium phosphate bone cement: in vivo evaluation with regard to application as injectable biological bone substitute.,” Cells. Tissues. Organs, vol. 179, no. 4, pp. 158–69, 7 2005. [PubMed: 16046862]

[20]. Piard CM, Chen Y, and Fisher JP, “Cell-Laden 3D Printed Scaffolds for Bone Tissue Engineering,” Clin. Rev. Bone Miner. Metab, vol. 13, no. 4, 2015.

[21]. Gunatillake PA and Adhikari R, “Biodegradable synthetic polymers for tissue engineering.,” Eur. Cell. Mater, vol. 5, p. 1–16; discussion 16, 5 2003. [PubMed: 14562275]

[22]. Roohani-Esfahani S-I, Newman P, and Zreiqat H, “Design and Fabrication of 3D printed Scaffolds with a Mechanical Strength Comparable to Cortical Bone to Repair Large Bone Defects,” Scientific Reports, vol. 6, pp. 19468, 1 2016. [PubMed: 26782020]

[23]. KARAGEORGIOU V and KAPLAN D, “Porosity of 3D biomaterial scaffolds and osteogenesis,” Biomaterials, vol. 26, no. 27, pp. 5474–5491, 9 2005. [PubMed: 15860204]

[24]. Cyster LA, Grant DM, Howdle SM, Rose FRAJ, Irvine DJ, Freeman D, Scotchford CA, and Shakesheff KM, “The influence of dispersant concentration on the pore morphology of hydroxyapatite ceramics for bone tissue engineering,” Biomaterials, vol. 26, no. 7, pp. 697–702, 3 2005. [PubMed: 15350773]

[25]. Kirkpatrick CJ, Fuchs S, and Unger RE, “Co-culture systems for vascularization — Learning from nature,” Adv. Drug Deliv. Rev, vol. 63, no. 4–5, pp. 291–299, 4 2011. [PubMed: 21281686]

[26]. Kolbe M, Xiang Z, Dohle E, Tonak M, Kirkpatrick CJ, and Fuchs S, “Paracrine Effects Influenced by Cell Culture Medium and Consequences on Microvessel-Like Structures in Cocultures of Mesenchymal Stem Cells and Outgrowth Endothelial Cells,” Tissue Eng. Part A, vol. 17, no. 17–18, pp. 2199–2212, 9 2011. [PubMed: 21529248]

[27]. Gershovich JG, Dahlin RL, Kasper FK, and Mikos AG, “Enhanced Osteogenesis in Cocultures with Human Mesenchymal Stem Cells and Endothelial Cells on Polymeric Microfiber Scaffolds,” Tissue Eng. Part A, vol. 19, no. 23–24, pp. 2565–2576, 12 2013. [PubMed: 23799306]

[28]. Huang Z, Ren P-G, Ma T, Smith RL, and Goodman SB, “Modulating osteogenesis of mesenchymal stem cells by modifying growth factor availability.,” Cytokine, vol. 51, no. 3, pp. 305–10, 9 2010. [PubMed: 20580248]

[29]. Ern C, Krump-Konvalinkova V, Docheva D, Schindler S, Rossmann O, Böcker W, Mutschler W, and Schieker M, “Interactions of Human Endothelial and Multipotent Mesenchymal Stem Cells in Cocultures,” Open Biomed. Eng. J, vol. 4, no. 1, pp. 190–198, 3 2010. [PubMed: 21625373]

[30]. Guerrero J, Catros S, Derkaoui S-M, Lalande C, Siadous R, Bareille R, Thébaud N, Bordenave L, Chassande O, Le Visage C, Letourneur D, and Amédée J, “Cell interactions between human progenitor-derived endothelial cells and human mesenchymal stem cells in a three-dimensional macroporous polysaccharide-based scaffold promote osteogenesis,” Acta Biomater, vol. 9, no. 9, pp. 8200–8213, 9 2013. [PubMed: 23743130]

[31]. Su N, Gao P-L, Wang K, Wang J-Y, Zhong Y, and Luo Y, “Fibrous scaffolds potentiate the paracrine function of mesenchymal stem cells: A new dimension in cell-material interaction,” Biomaterials, vol. 141, pp. 74–85, 10 2017. [PubMed: 28667901]

[32]. Martín-Saavedra F, Crespo L, Escudero-Duch C, Saldaña L, Gómez-Barrena E, and Vilaboa N, “Substrate Microarchitecture Shapes the Paracrine Crosstalk of Stem Cells with Endothelial Cells and Osteoblasts,” Sci. Rep, vol. 7, no. 1, p. 15182, 12 2017. [PubMed: 29123118]

[33]. Kusuma GD, Carthew J, Lim R, and Frith JE, “Effect of the Microenvironment on Mesenchymal Stem Cell Paracrine Signaling: Opportunities to Engineer the Therapeutic Effect,” Stem Cells Dev, vol. 26, no. 9, pp. 617–631, 5 2017. [PubMed: 28186467]

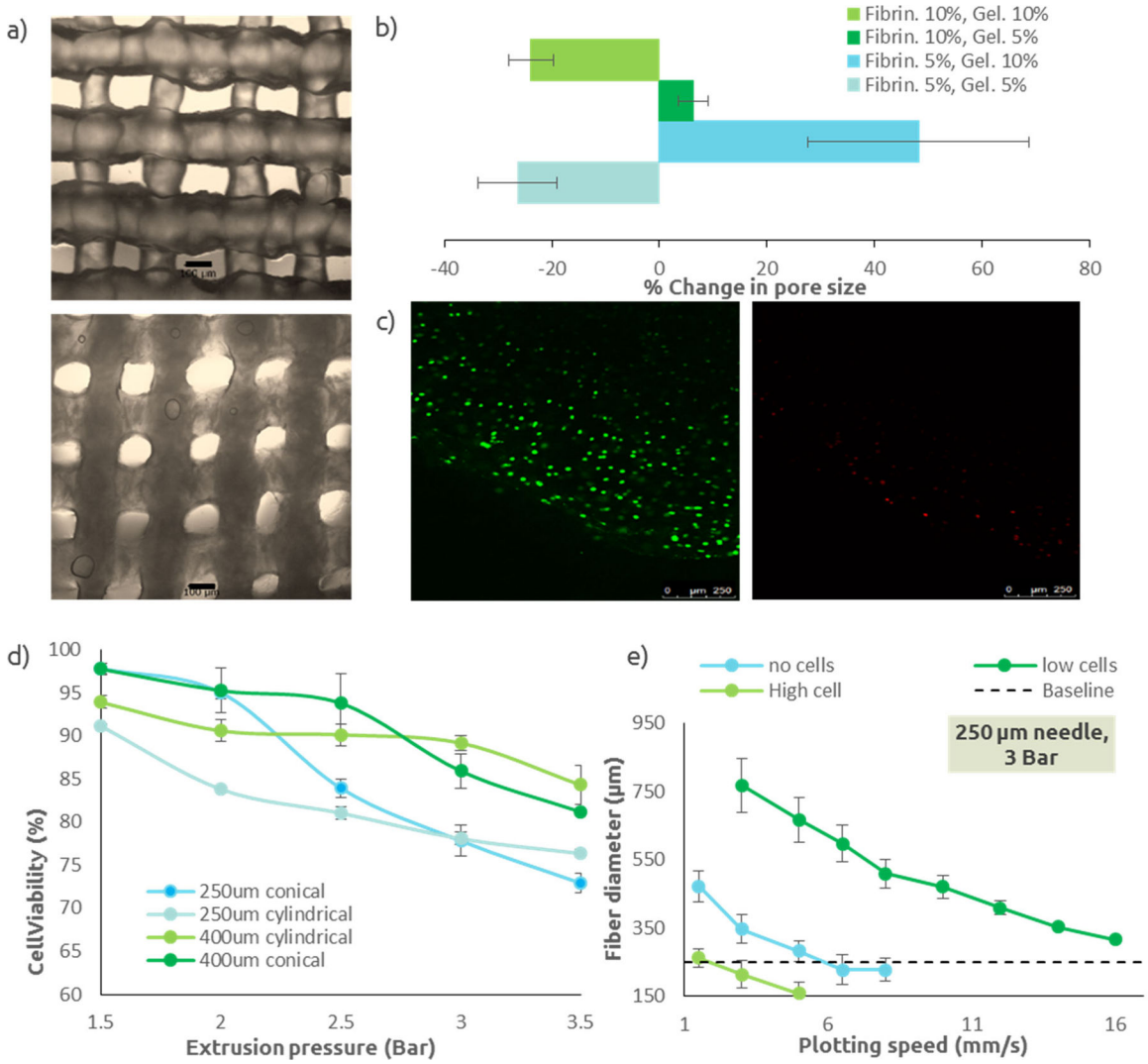

Figure I: Fibrin bioink characterization.

(a) Micrographs of 3D printed fibrin bioink (fibrinogen 5%, gelatin 5%) immediately after printing (top) and after 24h, following crosslinking of the fibrinogen and leaching of the gelatin (bottom). Fiber swelling is visible in this example. Scale bar is 100 µm. (b) Change in pore size for each bioink groups (n=9). A negative changes correlates to a swelling of the extruded fibers, while a positive change correspond to a shrinking of the extruded fibers. Fibrinogen 10%w/v/ gelatin 5%w/v was the chosen bioink composition for following experiments. (c) Live/Dead images of extruded L929. Live cells (left) are stained green, dead cells (right) are stained red. Cells were counted using Image J in order to quantify cell viability. (d) Cell viability after extrusion in the 3D printer, as a function of extrusion pressure and needle size/shape (n=6). (e) Extruded fiber diameter as a function of extrusion pressure, plotting speed, and cell density for a needle with an inner diameter of 250µm, which was used in following experiments (n=9). The baseline line represent the targeted fiber diameter (i.e. needle inner diameter). All data points represent mean +/− standard deviation.

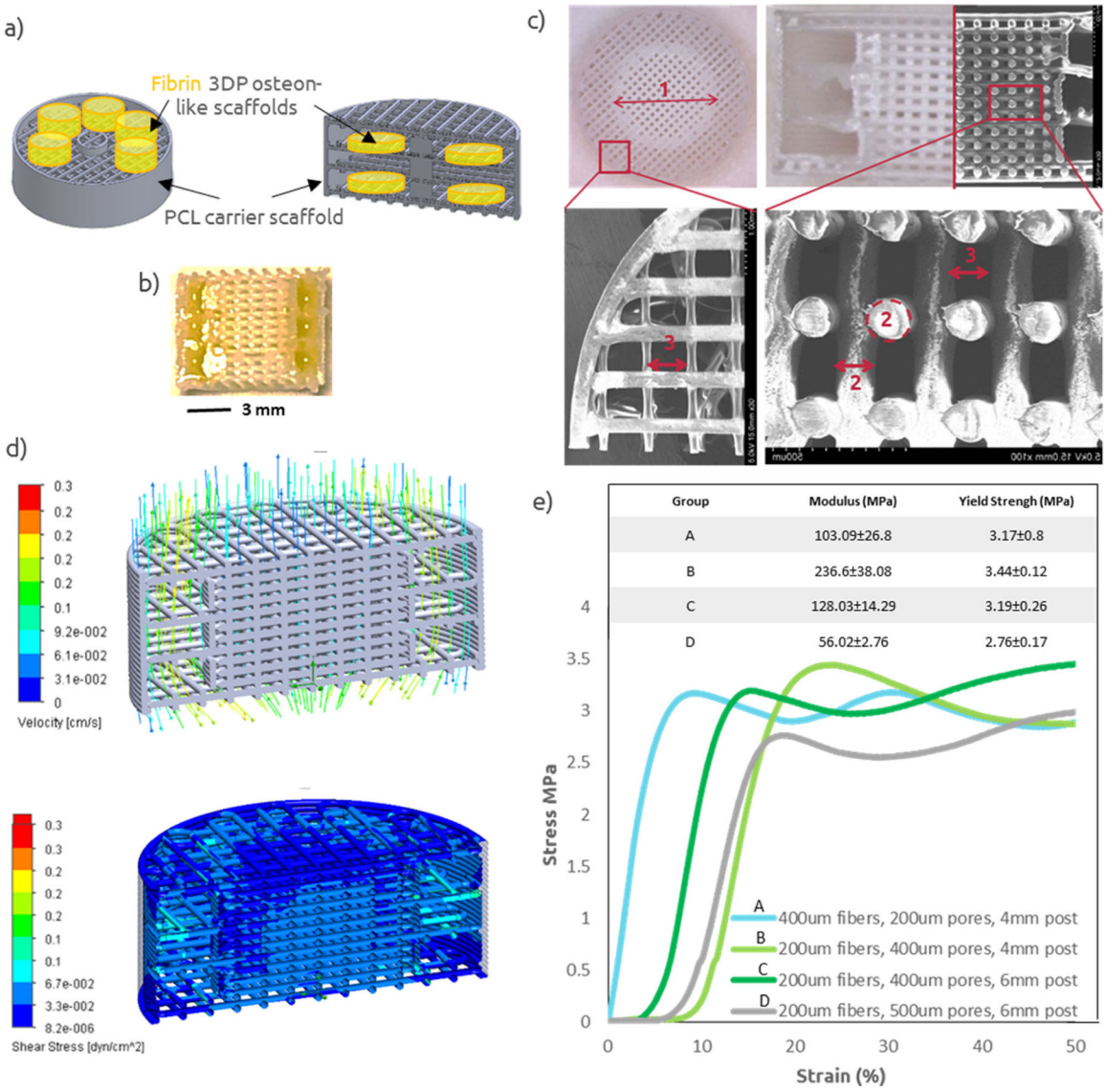

Figure II: PCL Carrier Scaffold Characterization.

(a) Schematic of 3D printed osteon-like scaffolds (green) and PCL carrier scaffold (gray). (b) Micrograph of a 3D printed PCL/Fibrin scaffold. Yellow food coloring was added to the fibrin bioink for photography purpose. (c) Micrograph and SEM images of 3D printed PCL scaffolds, with variable central post diameter (1), fiber diameter (2), and pore size (3). (d) Computational modeling of flow and shear stress within 3DP scaffolds while under perfusion. (e) strain-stress curve for four representative examples of 3DP PCL scaffolds (n=4). All data points represent mean +/− standard deviation.

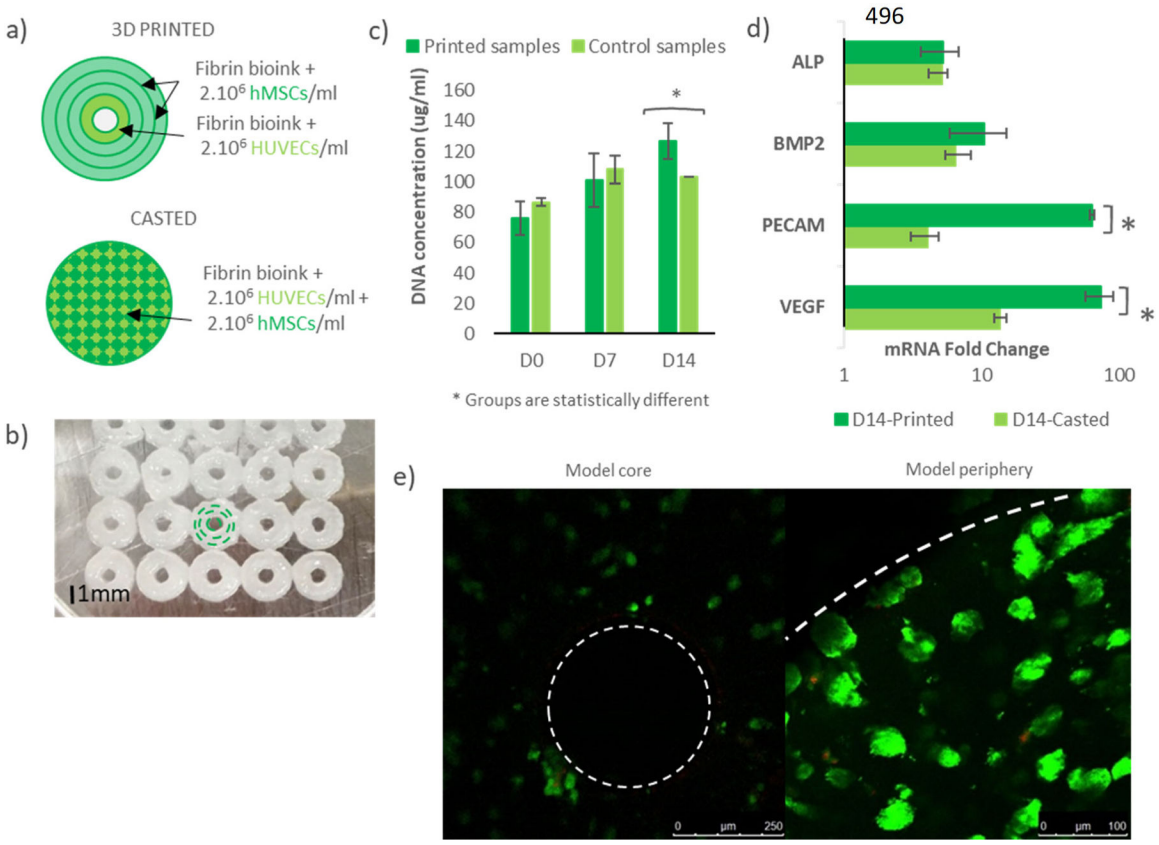

Figure III: Osteon-like scaffolds in-vitro experiment.

(a) Schematic of 3D printed osteon-like scaffolds and casted controls. 3DP scaffolds are composed of four concentric fibrin fibers of 250µm in diameter, containing hMSCs for the three outermost rings, and HUVECs for the innermost ring. Casted samples containing a mixture of MSCs and HUVECs (2.10^6 cells/ml) were used as controls. (b) Bioplotter picture of 3D printed constructs. The inner channel is 350µm in diameter and the complete scaffold is 2.5 mm in diameter. (c) DNA quantification assay showed significant increase in DNA concentration ($p<0.05$) over 14 days of *in vitro* culture in the printed samples compared to the casted samples (n=9). In addition, a significant higher DNA concentration ($p<0.05$) was shown in the printed samples, while the casted samples showed no significant changes. (d) mRNA expression fold change between day 0 and day 14 of *in vitro* culture (n=9). Rt-PCR showed no significant difference in gene expression of osteogenic markers ($p=0.098$), but a significant fold change in mRNA of angiogenic markers ($p<0.05$). (e) Live/Dead images of 3D printed scaffolds at day 14 (n=3). Live cells are stained green, and dead cells are stained red. Cells were counted using Image J in order to quantify cell viability. All data points represent mean +/− standard deviation.

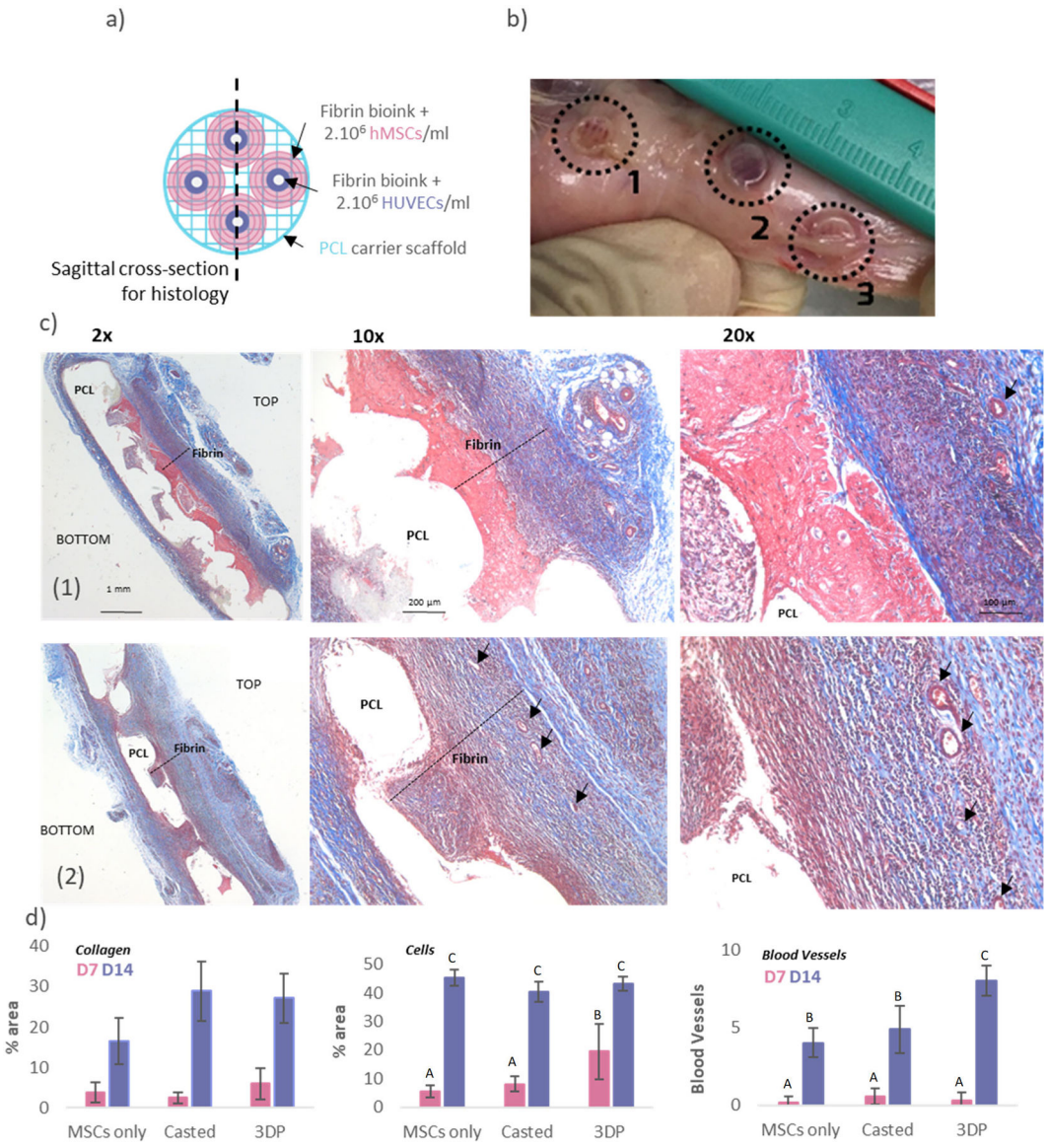

Figure IV: Osteon-like scaffolds in-vivo experiments.

(a) Schematic of a 3DP scaffolds. Osteon-like fibrin hydrogels are co-printed with PCL for support. Each 3DP sample comprises four osteon-like fibrin hydrogels, with a diameter of 6.4mm. Control samples consisted of fibrin bioink casted within the barrel of a 3 mm diameter syringe. Once gelled, control samples were casted out of the syringe using the plunger and assembled onto a 3D printed PCL scaffold. (b) Images of samples after 14 days implantation *in vivo*. TOP refers to the side of the implant with osteons, while BOTTOM refers to the side with the PCL support. (1) rMSCs only control scaffold, (2) rMSCs/RAECs control casted scaffold, and (3) rMSCs/RAECs 3DP osteon-like scaffold. (c) Micrographs of embedded, sectioned and stained samples using Masson Trichrome. Line (1) images of rMSCs/RAECs controls at day 14 after implantation. Line (2) images of 3DP rMSCs/RAECs at day 14 after implantation. Collagen is stained blue, cell nuclei are stained dark purple and fibrin is stained pink. Black arrows indicate blood vessels. (d) Quantitative

analysis of Masson's Trichrome images showing the percent area of the pictures covered by either collagen or cells, and the average number of blood vessels per picture (n=12). All data points represent mean +/− standard deviation. Groups not sharing a letter are statistically different ($p<0.05$).